Arch. Mech., 42, 3, pp. 279–289, Warszawa 1990

Dislocations and disclinations in a new light

M. J. MARCINKOWSKI (MARYLAND)

THE CONVENTIONAL treatments of the interrelationships between dislocations, disclinations, disclination dipoles and grain boundaries have been re-examined in detail and shown to contain a number of serious inconsistencies. When the concept of surface dislocations is introduced into the classical analysis, however, these difficulties are immediately eliminated and a new richness emerges from the theory.

Szczegółowo przeanalizowano ponownie tradycyjne ujęcie związków między dyslokacjami, dipolami dysklinacyjnymi oraz granicami ziaren, stwierdzając szereg istotnych niekonsekwencji w tym ujęciu. Znikają one natychmiast po wprowadzeniu pojęcia dyslokacji powierzchniowych, co prowadzi do istotnego wzbogacenia całej teorii.

Подробно проанализирован вновь традиционный подход к соотношениям между дислокациями, дисклинациями, дисклинационными диполями и границами зерен, констатируя ряд существенных непоследовательностей в этом подходе. Они исчезают мгновенно после введения понятия поверхностных дислокаций, что приводит к существенному обогащению целой теории.

1. Introduction

A CLOSE GEOMETRICAL relationship has been shown to exist between lattice dislocations, surface dislocations, disclinations and grain boundaries [1]. It has also been demonstrated by DE WIT that a close mathematical relationship exists between the theory of dislocations and disclinations [2]; however, the concept of surface dislocations is not contained therein. It will therefore be the purpose of this study to bring forth a greater unity between the physics and mathematics that underlie the close interrelationship between these various types of defect.

2. Disclinations and continuous dislocation distributions

Consider first the simple quantized edge-type lattice dislocation shown in Fig. 1a. The components of stress associated with this dislocation may be written as [3]

$$\sigma_{xx} = -\frac{\mu b}{2\pi(1-\nu)}\frac{y(3x^2+y^2)}{(x^2+y^2)^2},$$

$$\sigma_{yy} = \frac{\mu b}{2\pi(1-\nu)}\frac{y(x^2-y^2)}{(x^2+y^2)^2}, \tag{2.1}$$

$$\sigma_{xy} = \frac{\mu b}{2\pi(1-\nu)}\frac{x(x^2-y^2)}{(x^2+y^2)^2},$$

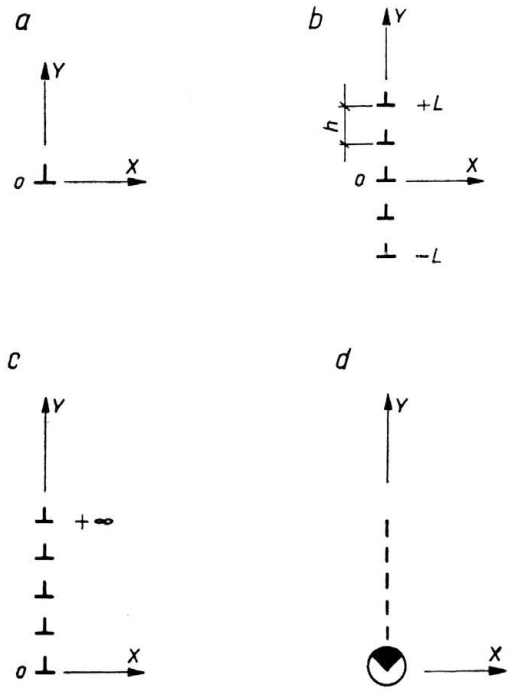

FIG. 1. a) Single, b) vertical wall of edge-type dislocation, c) dislocation representation of the wedge disclination in d).

where μ is the shear modulus, b—the Burgers vector of the dislocation, and ν is Poisson's ratio. The fourth component of stress can be readily obtained from the following relation:

$$\sigma_{zz} = \nu(\sigma_{xx}+\sigma_{yy}). \tag{2.2}$$

A uniform distribution of a finite number of vertical lattice dislocations with nearest-neighbor spacing h yields the finite wall of length $2L$ shown in Fig. 1b. Assuming this discrete array of dislocations to be continuously distributed, Eqs. (2.1) can be rewritten as [4, 5]

$$\begin{aligned}
\sigma_{xx} &= -\frac{\mu b}{2\pi(1-\nu)h}\int_{-L}^{L}\frac{(y+y')[3x^2+(y+y')^2]dy'}{[x^2+(y+y')^2]^2},\\
\sigma_{yy} &= \frac{\mu b}{2\pi(1-\nu)h}\int_{-L}^{L}\frac{(y+y')[x^2-(y+y')^2]dy'}{[x^2+(y+y')^2]^2},\\
\sigma_{xy} &= \frac{\mu b}{2\pi(1-\nu)h}\int_{-L}^{L}\frac{x[x^2-(y+y')^2]dy'}{[x^2+(y+y')^2]^2}.
\end{aligned} \tag{2.3}$$

The above equations can be readily integrated to yield [6]

$$\sigma_{xx} = \frac{\mu b}{2\pi(1-\nu)h}\left[\frac{1}{2}\ln\frac{x^2+(y-L)^2}{x^2+(y+L)^2}+\frac{x^2}{x^2+(y+L)^2}-\frac{x^2}{x^2+(y-L)^2}\right], \tag{2.4}$$

$$(2.4)\ [\text{cont.}] \qquad \sigma_{yy} = \frac{\mu b}{2\pi(1-\nu)h}\left[\frac{1}{2}\ln\frac{x^2+(y-L)^2}{x^2+(y+L)^2} + \frac{x^2}{x^2+(y-L)^2} - \frac{x^2}{x^2+(y+L)^2}\right],$$

$$\sigma_{xy} = \frac{\mu b x}{2\pi(1-\nu)h}\left[\frac{y+L}{x^2+(y+L)^2} - \frac{y-L}{x^2+(y-L)^2}\right].$$

Consider the case in which $L \Rightarrow R$, where R is the radius of the body, and where $R \gg x, y$. Furthermore, let $-L \Rightarrow L$, i.e., the condition where the bottom of the dislocation wall lies along the positive y-axis. Equation (2.4) then become

$$\sigma_{xx} = \frac{\mu\Omega}{2\pi(1-\nu)}\left[\frac{1}{2}\ln\frac{x^2+(y+L)^2}{R^2} + \frac{x^2}{R^2} - \frac{x^2}{x^2+(y+L)^2}\right],$$

$$(2.5) \qquad \sigma_{yy} = \frac{\mu\Omega}{2\pi(1-\nu)}\left[\frac{1}{2}\ln\frac{x^2+(y+L)^2}{R^2} + \frac{x^2}{x^2+(y+L)^2} - \frac{x^2}{R^2}\right],$$

$$\sigma_{xy} = \frac{\mu\Omega x}{2\pi(1-\nu)}\left[\frac{1}{R} - \frac{y+L}{x^2+(y+L)^2}\right].$$

The above equations represent the stress field of a wedge disclination located at the position L within a finite body of dimensions R. The wedge angle Ω associated with this disclination can be written as

$$(2.6) \qquad \Omega = \frac{b}{h}.$$

Compared to the stress field expressions for an edge dislocation given by Eqs. (2.1), those associated with a wedge disclination are relatively complex since, as Eqs. (2.5) show, they depend on both R and L. They may be simplified somewhat by placing the disclination at the center of the body; i.e., letting $L = 0$. Further simplification occurs by allowing the body to become infinite, which corresponds to letting $R = \infty$. Equations (2.5) thus become

$$\sigma_{xx} = -\infty,$$

$$(2.7) \qquad \sigma_{yy} = -\infty,$$

$$\sigma_{xy} = -\frac{\mu\Omega xy}{2\pi(1-\nu)(x^2+y^2)},$$

which corresponds to the configuration depicted in Fig. 1c. This wedge disclination is represented again in a nondislocation manner by the circle and dark wedge symbol in Fig. 1d. It was VOLTERRA [7] who first proposed the six basic types of distortion. One of them was the edge dislocation and another the wedge disclination. It has been reasoned that the uniqueness of the disclination lies in its rotational character in contrast to the translational nature of the dislocation [2]. However, to the extent that a disclination can be represented in terms of an array of dislocations, this uniqueness is eliminated so that only the pre-eminence of the dislocation is maintained. This pre-eminence will be made even sharper in the following sections when the concept of a grain boundary is discussed. In principle, however, it should be possible to arrive at the same stress fields for a disclination whether one uses the non-dislocation model of Fig. 1d or the dislocation model

of Fig. 1c. Utilizing the former approach, DE WIT [2] was able to obtain an expression for σ_{xy} analogous to Eq. $(2.7)_3$. Since he was also dealing with an infinite body, his equations corresponding to σ_{xx} and σ_{yy} should have also reduced to the same infinite values given by Eqs. $(2.7)_1$ and $(2.7)_2$, which they do not. The reason for the present results is that the logarithmic terms in Eqs. $(2.5)_1$ and $(2.5)_2$ increase without limit as R in the denominators increase without limit. This is a physically reasonable result since the dilatational stresses would be expected to become infinite as the extra matter associated with the dislocation wall approaches infinity. The fact that this result is not reflected in De Wit's stress field expressions may be related to his stated omission of all those terms in his preparatory equations that gave rise to infinities.

3. Disclination dipoles

In the limiting case where $L = \infty$ and $-L = -\infty$, the infinite wall of uniformly spaced edge type dislocations shown in Fig. 2a is obtained. When these dislocations are

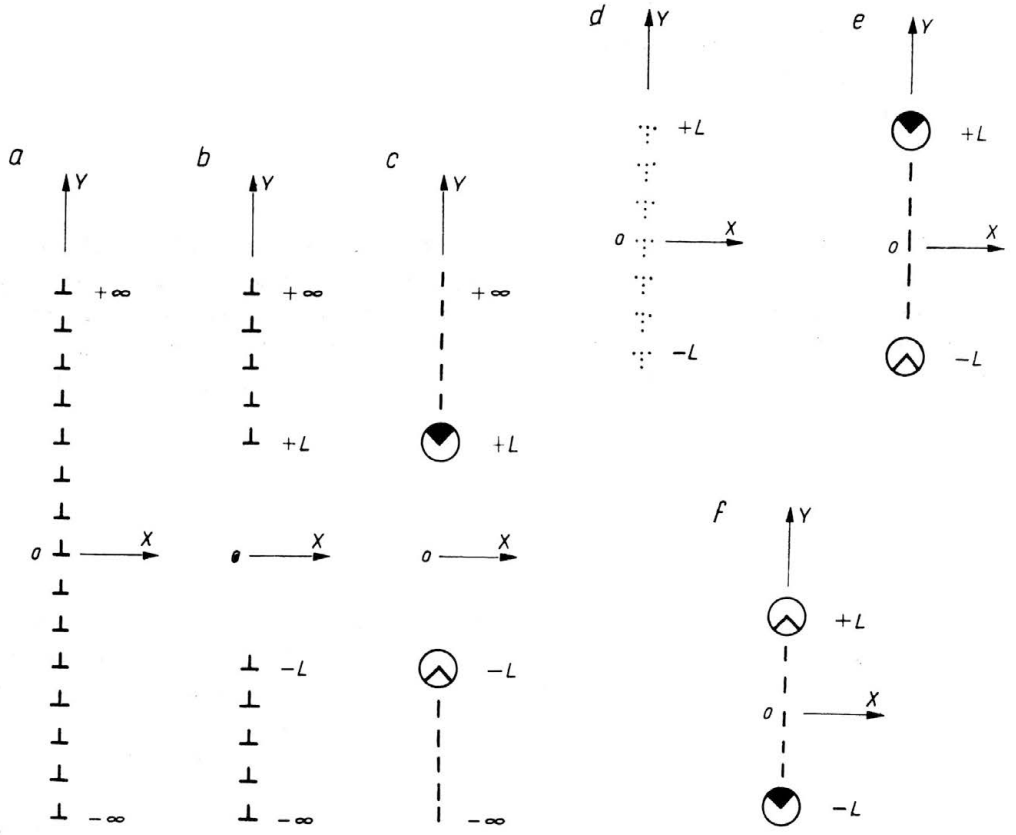

FIG. 2. a) Vertical wall of uniformly spaced edge dislocations, b) configuration obtained after removal of dislocations over a length $2L$ in a), c) disclination dipole representation of b), d) surface dislocation representation of configuration in b), e) disclination dipole model of d), f) disclination representation of Fig. 1b.

continuously distributed, Eqs. (2.4) can be used to arrive at the following results:

$$\sigma_{xx} = \sigma_{yy} = \sigma_{xy} = 0. \tag{3.1}$$

The vanishing of these stresses is the cornerstone of the conventional, albeit incorrect belief, that the dislocation configuration of Fig. 2a corresponds to the correct representation of a grain boundary [3–6]. In fact, the results of Eq. (3.1) are in surprising contradiction to the findings of Eqs. (2.7) for a semi-infinite wall of dislocations. In particular, it is intuitively obvious that the dilatational stresses must approach infinity as both $y \to \infty$ and $y \to -\infty$ in Fig. 2a, as was also argued to be the case for the semi-infinite wall of Fig. 1c. The seeming contradiction between the results of Eqs. (2.7) and Eq. (3.1) arises from the fact that the latter were obtained by assuming $L \gg x, y$ in Eqs. (3.1), so that in the limit where $L \to \infty$, they represent the stress at the center of an infinite wall of dislocations only [8]. At large distances from the center, Eq. (3.1) no longer holds, so that the wall in Fig. 2a generates long-range stresses.

If now a portion of the dislocations in Fig. 2a that lie within a region $2L$ at the center of the wall is removed, the configuration depicted in Fig. 2b is obtained. Application of Eqs. (2.4) to this configuration yields

$$\begin{aligned} \sigma_{xx} &= -\sigma'_{xx}, \\ \sigma_{yy} &= -\sigma'_{yy}, \\ \sigma_{xy} &= -\sigma'_{xy}, \end{aligned} \tag{3.2}$$

where σ'_{xx}, etc. simply denote the stresses given by Eq. $(2.4)_1$ etc. The negative sign indicates that the configuration of Fig. 2b corresponds to that of a finite wall of dislocations of length $2L$, such as depicted in Fig. 1b, but of opposite sign, as shown in Fig. 2d. The dislocations are drawn dotted in this figure to differentiate them from the extra matter dislocations which were the original source of the distortion. These will be termed surface dislocations for reasons that will be made clear later.

Extending the reasoning obtained in connection with Figs. 1c and 1d to Fig. 2b, it follows that the latter configuration can also be represented in terms of a pure wedge disclination dipole, as illustrated in Fig. 2c. The disclination, symbolized by the light wedge, simply represents the material that was removed, as contrasted to the dark wedge which corresponds to extra matter [9]. Application of the wedge disclination expressions given by Eqs. (2.5) to Fig. 2c, where the sign of Ω is taken as negative for the lowermost disclination, yields the same results as those given by Eqs. (3.2), as expected. It also follows that the dislocation configuration in Fig. 2d can be alternately represented as a disclination dipole, such as depicted in Fig. 2b, which is in turn identical to the disclination dipole of Fig. 2c. This result is to be expected since both configurations are identical. In a similar fashion, the finite wall of dislocations shown in Fig. 1b can be represented in terms of the wedge disclination dipole illustrated in Fig. 2f. It is clear that this dipole is of opposite sense to that in Fig. 2e, i.e., rotated by 180°. It is a relatively straightforward procedure to apply the disclination stress field Eqs. (2.5) to the configuration in Fig. 2f to obtain the results given by Eqs. (2.4). Application of DEWIT's [2] disclination stress field equations to this configuration yields results similar to Eqs. (2.4) (see his

(Eqs. 9.6)) but with x^2 and $-x^2$ in Eq. $(2.4)_1$ replaced by $-(y+L)^2$ and $+(y-L)^2$ respectively, and presumably arises from his discrepancies with Eqs. (2.7) mentioned earlier.

Consider next the vertical wall of disclination dipoles illustrated in Fig. 3a. It is clear from reference to Figs. 2e and 2f that this array may be depicted alternately in terms of a nonuniform array of lattice and surface dislocations, as shown in Fig. 3b. LI [10] has in fact used the representation in Fig. 3a to describe the structure of grain boundaries; however, he incorrectly interprets Fig. 3a in terms of only the single array of lattice dislocations in Fig. 3b, apparently unaware of the concept of surface dislocations. For rea-

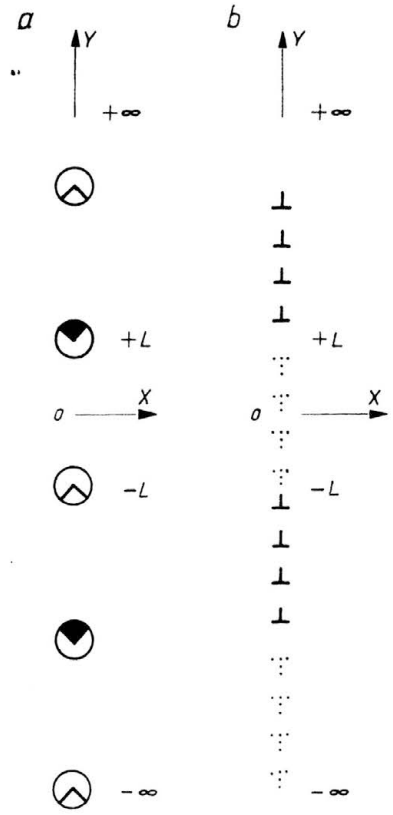

FIG. 3. a) Vertical wall of disclination dipoles, b) alternate representation of a) in terms of lattice and surface dislocations.

sons similar to that given in connection with Fig. 2a, the omission of the surface dislocations in Fig. 3b would generate enormous long-range stresses. LI [10] then writes the energy of the dipole array in Fig. 3a in terms of a single finite wall of edge dislocations such as shown in Fig. 1b to obtain

$$E = \frac{\mu\Omega^2 L^2}{\pi(1-\nu)} \ln \frac{R}{2L}, \tag{3.3}$$

where $R \gg L$. This is clearly an unacceptable result since E becomes infinite as R approaches infinity; i.e., the same result obtained for a single dislocation within an infinite body.

4. Dislocation walls in terms of surface dislocations

It has been shown conclusively that the classical model of grain boundaries first proposed by BURGERS [11], based upon a single wall of lattice dislocations, such as depicted in Fig. 2a, is incomplete [12–15]. In order to eliminate the long-range stresses associated with such a boundary, it is necessary to incorporate into it a continuous distribution of surface dislocations, such as shown in Fig. 4a. These surface dislocations are denoted by

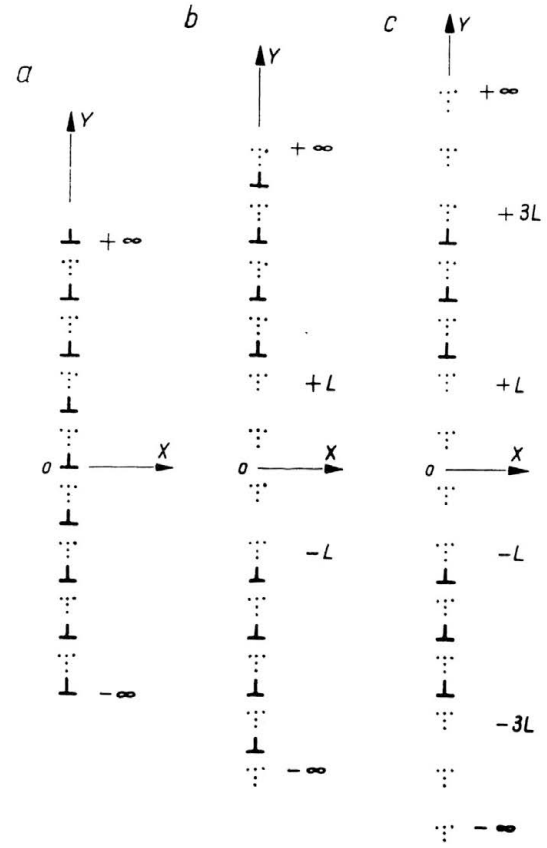

FIG. 4. a) Vertical wall of uniformly spaced edge-type lattice and surface dislocations, b) configuration obtained after removal of lattice dislocations over a length 2L in a), c) same as b) but with periodic removal of lattice dislocations over intervals of $2L$.

dotted symbols and possess Burgers vectors opposite in sign to those of the lattice dislocations. To a good approximation, then, the grain boundary may be visualized as a periodic array of dislocation dipoles. It therefore follows that the lattice and surface dislocations obey the following powerful conservation law [16]:

$$\Sigma b_L + \Sigma b_s = 0, \tag{4.1}$$

where the subscripts L and s denote lattice and surface dislocations, respectively. It is thus the dipole nature of the grain boundary that insures the vanishing of long-range stresses and therefore low energy.

The energy of a grain boundary can be written as

$$E = \frac{b}{2h} \int_0^x \sigma_{xy} dx, \tag{4.2}$$

where the expression used for σ_{xy} in the above integral has customarily not been the general one given by Eq. $(2.4)_3$, but one analogous to $\sigma_{xy} = 0$ given by Eq. (3.1). Strictly speaking these authors used the expression for σ_{xy} obtained from an infinite wall of discrete lattice dislocations. The general results were nevertheless the same, namely that Eq. (4.2) yielded a very low value for the grain boundary energy. As mentioned earlier, however, the results expressed by Eqs. (3.1) are not general. In order to incorporate this generalization into Eq. (4.2), let us consider Eq. $(2.4)_3$ for the case where $y = 0$ to obtain

$$\sigma_{xy} = \frac{\mu b}{\pi(1-\nu)h} \frac{xL}{x^2+L^2}, \tag{4.3}$$

substituting this result into Eq. (4.2) and integrating gives

$$E = \frac{\mu b^2 L}{2\pi(1-\nu)h^2} \ln \frac{(x^2+L^2)}{L^2}. \tag{4.4}$$

Letting $x = L$, i.e., the length of the grain boudary being of the order of the size of the body, we find

$$E = \frac{\mu b^2 L \ln 2}{2\pi(1-\nu)h^2} \tag{4.5}$$

which, for an infinite body, i.e., $L = \infty$, yields $E = \infty$. We thus arrive at a result which is just the opposite of that obtained from the conventional theory [3–6], giving yet another reason to reject the model of a grain boundary in Fig. 2a portrayed in terms of a single wall of lattice dislocations.

If the lattice dislocations are removed from the center of the grain boundary in Fig. 4a over a length $2L$, the configuration illustrated in Fig. 4b is obtained. In particular, the surface dislocations, which originally formed dipoles with the removed lattice dislocations, are left behind at their original positions within the grain boundary. These surface dislocations were originally thought to be basically distinct from lattice dislocations and were therefore given the name of virtual dislocation [17]. This problem was later resolved when it was demonstrated that the surface dislocation could be visualized in terms of another geometrical representation based upon the coincidence site lattice [18]. Comparison of Fig. 4b with Fig. 2b, or its equivalent in Fig. 2d, however, shows that they are not identical, since in the former case the segments of the wall from L to ∞ and $-L$ to $-\infty$ generate no long-range stresses, whereas those in Fig. 2b do. On the other hand, since these long-range stresses are screened from the center of the wall in Fig. 2b, Eqs. (3.2) can be used to represent the stress fields of the configurations in either Fig.

2b, 2d or 4b. At the same time, in view of the prohibitively high energy of the dislocation wall in Fig. 2b compared to that in Fig. 4b, the former must be ruled out as ever being physically realizable.

If now lattice dislocations are removed from the grain boundary of Fig. 4a in a periodic manner, such as illustrated in Fig. 4c, the resulting structure will become unstable because of the generation of large long-range stresses. These stresses can be eliminated by allowing the surface dislocations that are coupled with the remaining lattice dislocations to move out of the boundary so as to generate the relatively low energy configuration of Fig. 3b, or its disclination dipole counterpart in Fig. 3a.

Assuming the dislocation dipole spacing in Fig. 4a to be L, the energy of the boundary can be determined to be the sum of the self and interaction energies of each dipole to yield

$$E = \frac{\mu b^2}{2\pi(1-\nu)L} \ln \frac{L}{r_0}, \tag{4.6}$$

where r_0 is the dislocation core or cut-off radius. In contrast to Eq. (3.3) the above relation shows the grain boundary energy to be a function of the dislocation dipole spacing only.

Comparison of Figs. 3b and 4a shows that in the limit of small values of L, both configurations are essentially identical, so that the grain boundary of Fig. 4a could also be viewed as an array of disclination dipoles. However, since the disclination is a derived quantity, i.e., derivable from a specific dislocation array, it is dangerous to rely on the disclination dipole model alone in those cases where a more accurate description of the grain boundary could be obtained in terms of surface and lattice dislocations [12–15].

5. Dislocation walls within finite bodies

We have not yet considered the surface effects on the various dislocation and disclination arrays discussed thus far. It will now be shown that these considerations can be significant. In the case where the size of the body R is large compared to the length of the finite wall L in Fig. 1b, we obtain the configuration shown in Fig. 5a. In order to satisfy the stress-free boundary conditions, it is necessary to distribute a continuous array of surface dislocations on the surface of the body which satisfy Eq. (4.1) [16, 18]. The distribution of these surface dislocations in fact determines the shape of the outer surfaces of the finite body, as is evident in Fig. 5a.

In the case where the dislocation wall in Fig. 5a extends to the upper surface of the finite body, we obtain the wedge disclination configuration of Fig. 5b. This is the finite counterpart of Fig. 1c. Unlike the situation in Fig. 5a, L in Fig. 5b is on the order of R.

When the dislocation wall in Fig. 5a is allowed to extend to both the top and bottom faces of the finite body, the configuration shown in Fig. 5c is obtained. This is the finite counterpart of Fig. 2a. Unlike the two cases shown in Figs. 5a and 5b, it is not possible to arrange the surface dislocations on the surface so as to render it stress-free. Although the surface dislocations in Fig. 5c still obey Eq. (4.1), they generate surface stresses. These surface stresses are simply a realization of the fact that the finite body in Fig. 5c cannot be maintained in a state of equilibrium in the absence of external forces or tractions.

Upon removal of the surface tractions in Fig. 5c, the surface dislocations pair themselves with the lattice dislocations and form the grain boundary shown in Fig. 5d. It is

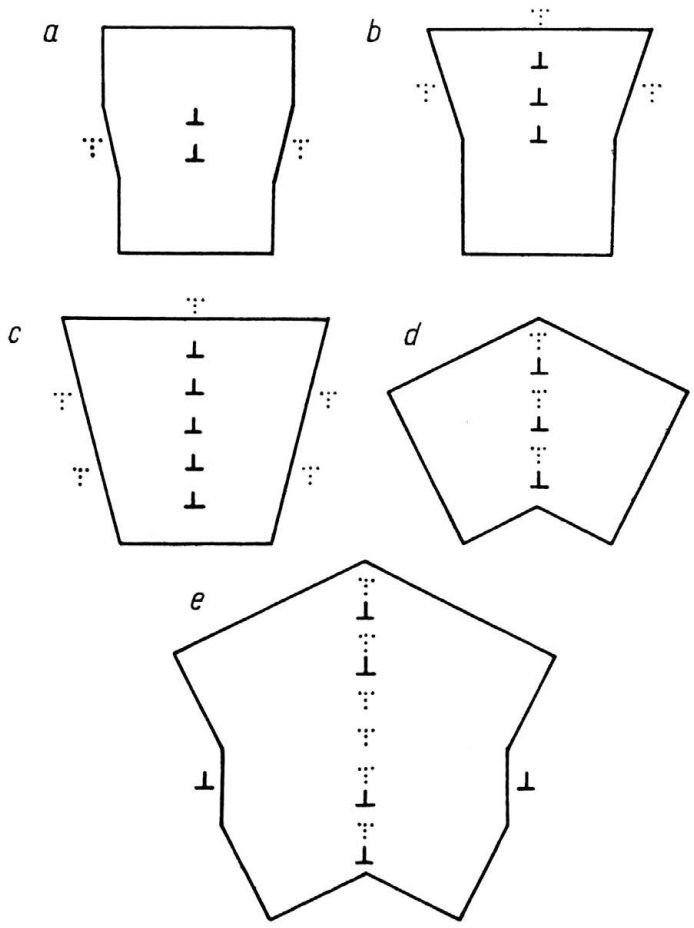

FIG. 5. a), b), c), d), e) Finite body representations of configurations in Figs. 1b, 1c, 2a, 4a and 4b, respectively.

clear that Fig. 5d is simply the finite body counterpart of Fig. 4a. Unlike the three cases depicted in Figs. 5a, 5b and 5c, the outer surfaces of Fig. 5d are entirely stress-free.

Finally, upon removal of a finite number of lattice dislocations from the center of the grain boundary in Fig. 5d, we obtain the configuration depicted in Fig. 5e which is simply the finite body counterpart of Fig. 4b. The surface dislocations on the outer surfaces of the body in Fig. 5e are drawn solid to indicate that they originated from lattice dislocations which were originally situated within the grain boundary. This interchange between surface and lattice dislocations underscores the close similarity between the two. It also follows that the surface dislocations in Fig. 5e render the outer surfaces of this body stress-free.

6. Summary and conclusions

The conventional theory of the interrelationship between dislocations and disclinations has been re-examined in detail and found to contain significant conceptual drawbacks. The root of the problem lies in the failure of the more classical approach to incorporate into it the concept of surface dislocations. This in turn has led such important defects as disclination dipoles and grain boundaries to be incorrectly interpreted in terms of lattice dislocations alone. In addition, various boundary conditions associated with certain dislocation and disclination arrays have been neglected in the conventional theories, in turn leading to serious misconceptions. These difficulties have been shown to vanish when surface dislocations are incorporated into the classical treatment.

References

1. M. J. MARCINKOWSKI, *The surface dislocation—a universal concept*, Phys. Stat. Sol. (a), **60**, 109–116, 1980.
2. R. DE WIT, *Theory of disclinations. IV. Straight disclinations*, J. Res. Nat. Bur. Std., **77A**, 607–658, 1973.
3. A. H. COTTRELL, *Dislocations and plastic flow in crystals*, Clarendon Press, Oxford 1953.
4. J. P. HIRTH, J. LOTHE, *Theory of dislocations*, McGraw-Hill, New York 1968.
5. S. AMELINCKX, W. DEKEYSER, *The structure and properties of grain boundaries*, in: Solid State Physics, 8, 325–499, F. SEITZ and D. TURNBULL [ed.], Academic Press, New York 1959.
6. J. C. M. LI, *Theory of strengthening by dislocation groupings*, in: Electron Microscopy and Strength of Crystals, 713–779, G. THOMAS and J. WASHBURN [ed.], Interscience, New York 1963.
7. V. VOLTERRA, *Sur l'équilibre des corps élastiques multiplement connexes*, Ann. Ecole. Norm. Supér., **24**, 400–420, 1907.
8. M. J. MARCINKOWSKI, *Grain boundaries revisited*, Phys. Stat. Sol., (a), **96**, 425–434, 1986.
9. M. J. MARCINKOWSKI, E. S. P. DAS, *A general analysis of the structure of simple tilt boundaries*, Phil. Mag., **26**, 1281–1300, 1972.
10. J. C. M. LI, *Disclination model of high angle grain boundaries*, Surface Science, **31**, 12–26, 1972.
11. J. M. BURGERS, *Some considerations on the fields of stress connected with dislocations in a regular crystal lattice. I*, Proc. Kong. Ned. Akad. Wet., **42**, 293–325, 1939.
12. M. J. MARCINKOWSKI, *Unified theory of grain bounduries: an update*, Phys. Stat. Sol., (a), **73**, 409–419, 1982.
13. M. J. MARCINKOWSKI, *A new approach to the theory of grain boundaries*, J. Mater. Sci., **18**, 827–839, 1983.
14. M. J. MARCINKOWSKI, *The role of surface dislocations in the continuum theory of lattice defects*, Phys. Stat. Sol., (b), **126**, 527–535, 1984.
15. M. J. MARCINKOWSKI, *The structure of twist boundaries in terms of surface dislocations*, Phys. Stat. Sol. (a), **88**, 129–136, 1985.
16. M. J. MARCINKOWSKI, *Unified theory of the mechanical behaviour of matter*, John Wiley and Sons, New York 1979.
17. M. J. MARCINKOWSKI, *Propagation of glide through internal boundaries*, in: Fundamental Aspects of Dislocation Theory, 531–545, J. A. SIMMONS, R. DE WIT and R. BULLOUGH [ed.], National Bureau of Standards, Washington D. C. 1970.
18. K. JAGANNADHAM, M. J. MARCINKOWSKI, *Surface dislocation model of a finite stressed solid*, J. Mat. Sci. and Eng., **38**, 259–270, 1979.

DEPARTMENT OF MECHANICAL ENGINEERING
UNIVERSITY OF MARYLAND, COLLEGE PARK, USA.

Received July 18, 1989.